Available online at www.sciencedirect.com
SCIENCE DIRECT®
Journal of Nuclear Materials 335 (2004) 366–378
journal of nuclear materials
www.elsevier.com/locate/jnucmat

Assessment of the constitutive properties from small ball punch test: experiment and modeling

E.N. Campitelli [a,*], P. Spätig [b], R. Bonadé [b], W. Hoffelner [a], M. Victoria [b]

[a] *Laboratory for Materials Behavior, Nuclear Energy and Safety Research Department, Paul Scherrer Institute, 5232 Villigen PSI, Switzerland*

[b] *Fusion Technology – Materials, CRPP – EPFL, Association EURATOM – Confederation Suisse, 5232 Villigen PSI, Switzerland*

Received 2 April 2004; accepted 20 July 2004

Abstract

An assessment of the true stress–true strain relationship has been done by means of tensile and small ball punch tests on austenitic and tempered martensitic steel at room temperature. A finite element model was developed and validated to calculate the force–deflection curve obtained from the ball punch experiment. The effects of the specimen thickness and material properties on the overall shape of the ball punch test curve are discussed. The constitutive behavior assigned to the specimen for the calculations was determined from the tensile test but we showed that assumptions have to be done to extend it to large strains as those arising during the punch tests. Using an inverse methodology, it was possible to show that a linear strain-hardening stage takes place at large strains. The potential for evaluating the evolution of the strain-hardening capacity after irradiation is outlined.

PACS: 62.20.Fe; 83.20.−d

1. Introduction

The use of small-scale specimen techniques for mechanical testing of irradiated materials is by now a worldwide spread interest. Over the last decades, numerous techniques applied on non-standard small specimens have been developed to extract a host of mechanical and physical properties. International symposia have been organized starting in 1986 [1] while reviews and recommendation for small specimen techniques have been continuously published e.g. [2–4]. There are mainly two reasons that drive the effort to develop and standardize this type of specimens, reasons that can be qualified as intrinsic and extrinsic. The intrinsic ones arise from limitations imposed by the standard scale testing techniques, for example: the availability of space in the irradiation facilities and the presence of fluence and/or irradiation temperature gradients for large samples. Another example is the technical impossibility of machining standard sized geometries out of commercial structural components like tubes or grids that were irradiated in-service and from which post-irradiation evaluation becomes mandatory. As example of the extrinsic reasons, we stress the need to reduce as much as possible the dose to personnel for post-irradiation testing.

* Corresponding author. Tel.: +41 56 310 21 89; fax: +41 56 310 45 29.
E-mail address: emiliano.campitelli@psi.ch (E.N. Campitelli).

0022-3115/$ - see front matter © 2004 Elsevier B.V. All rights reserved.
doi:10.1016/j.jnucmat.2004.07.052

Among the test techniques employed to characterize the constitutive behavior and the fracture properties of irradiated materials, the ball punch test has been extensively used [5–8]. For the time being, only test recommendations for small punch tests have been issued that are not always followed by the workers. Not even the same geometry for the experimental setup was used, and consequently, the resulting data sets are not directly comparable. In our opinion, the procedures for standard punch test of sheet metals described in ASTM standard E643-84 contain recommendations that can be applied to the smaller scale specimens used in this work (use of lubricant, etc.). On a phenomenological basis, correlations have been proposed, to extract from the punch tests, tensile test parameters like the yield stress, the ultimate tensile stress, the uniform elongation [9] or to estimate the ductile to brittle transition temperature [10]. In the same vein, different deformation stages have been associated to the ball punch curve but we shall show that, under certain circumstances, they contrast with the experimental results. To our judgment, there still remains some lack of understanding of the underlying mechanical processes that control the various calibration factors as well as their material and irradiation dependence. It has already been recognized that modeling with finite element calculations should become an inseparable tool for the correct interpretation of non-standard test curves [4] and a powerful and trustable method to estimate the correct constitutive parameters of the material. Finite element analysis was also used to calculate the stress state in punch specimen in order to interpret the crack appearance [11]. However, if one and the same FEM model is expected to provide valid calculations over a broad range of materials, it becomes mandatory to validate it performing simultaneously experiments and calculations on materials exhibiting significant differences in their mechanical behavior. A clear procedure along this line is still lacking. With the goal of completing a self consistent picture the following topics are addressed in this article:

- A finite element model and its validation are described.
- Results on tensile and punch tests on two types of steels (austenitic and tempered martensitic) are presented. We discuss the issues mentioned above (stages of deformation, validity of normalization procedures) under the light of the comparison between the calculated and the experimental force deflection curves.
- The combined effects of sample thickness, friction and material strength on the shape of the force deflection curves are discussed with the help of contour plots for the equivalent plastic strain provided by the FEM calculations.
- We show the adequacy of small ball punch testing in the estimation of the material strength for large deformations, an issue in which standard tensile tests may be of reduced applicability due to necking, especially for irradiated materials. In the case of irradiated materials where the plastic flow is often observed to be localized in dislocation channels, we discuss the possibility of using compression tests instead of tensile test to validate the methodology to determine the constitutive behavior.

2. Experimental procedures

2.1. Materials employed

Results of two technical stainless steels, with significantly different tensile properties (yield strength, strain-hardening and ductility) are presented in this study. These materials are a commercial, AISI type, austenitic 316L, and a tempered martensitic steel of the 7–9Cr class. The tempered martensitic alloy was produced in the framework of material development for fusion structural applications. It is a reduced activation tempered martensitic steel F82H-mod, heat E83697, produced by Böhler *AG*. This steel contains 7.65Cr–2.0W–0.1C–0.18V–0.04Ta and Fe for the balance. The steel was heat-treated by normalizing at 1253 K for 0.5 h and tempering at 1033 K for 1.5 h. The steel was fully martensitic after quenching [12,13]. The commercial 316L is a typical high creep strength, low corrosion austenitic steel with low carbon content. The nominal composition is 17Cr–12Ni–2.5Mo–2Mn–1Si–0.045P–0.03S–0.03C. This steel was provided by Stahag Stahl A.G, and was delivered in the standard 'annealed and cold drawn bar' condition.

2.2. Tensile tests

Tensile and small ball punch tests were performed at room temperature. DIN round specimens of 3 mm diameter and 18 mm in gauge length were used for tensile testing. The tensile tests were carried out with a Schenck RMC100 electro-mechanical testing machine at a constant crosshead velocity of 18 mm/min corresponding to a nominal strain-rate of $1.6 \times 10^{-2}\ s^{-1}$. This strain-rate was chosen since it approximately represents the averaged strain-rate that develops in the punch test specimens deformed according to the condition described below. Note that the strain-rate was found to have a well quantifiable effect on the strain-hardening rate of the tempered martensitic steel in particular [14], so it is very important to characterize the constitutive behavior with a strain-rate similar to that by which the disk is deformed. From the load-elongation data, the

true stress–true strain curves were calculated, so all the stresses and strains presented in this paper are expressed in true units. The elongation was measured with a clip gauge attached to the specimens.

2.3. Small ball punch tests

The ball punch tests were performed with a screw driven Zwick testing machine. The ball punch test essentially consists in deforming a center-loaded clamped disk with a spherical puncher; the load–displacement curve is then recorded. Details of our device are shown in Fig. 1(a), where the relevant dimensions are shown: the spherical puncher is a 0.5 mm radius (R1), hard steel ball of the type used in ball bearings. The ball is pushed by means of a rod trough a 1 mm hole in the upper die (D1) (a small tolerance of 0.05 mm and oil lubrication are necessary). The diameter of the hole on the lower die is 1.5 mm (D2), however, a carefully machined round billet radius of 0.2 mm (R2) is the interaction surface between the sample and the lower die. The sample (in black) is a disc of 3 mm diameter (D3) and a thickness varying between 0.23 and 0.27 mm approximately (T) (the depth of the step machined on the lower die should be slightly lower than the minimum thickness of the sample to be used, in such a way that the sample is well clamped when the two dies are screwed against each other). This type of sample geometry is expected to become widely used, not only because of the reduced size represents advances in the aforementioned intrinsic and extrinsic reasons, but also because it is at the same time the pre-sample for TEM observations. In this study, the displacement of the mobile traverse of the testing machine was recorded. It is then certainly necessary to deal with a compliance correction method (this will be described in Section 4.3). In future work it would be more adapted to avoid the compliance correction by measuring directly the displacement of the punch with a clip gauge system. The experimental set-up was designed according to the recommendations given in [3], where more details can be found. A constant displacement velocity of 1 mm/min for the steel ball was selected. This corresponds to a relatively high strain-rate. Keeping in mind that we intend to apply the ball punch testing for radioactive materials over a range of temperatures, temperature stability is always a matter of concern so that it is highly desirable to perform quick tests. Oil lubrication was used between the ball and the sample disk. The disks were extracted from a tensile specimen by cutting it perpendicularly to the gauge length by using a lubricated diamond saw. The disks were polished on both sides with a sequence of diminishing grit size silicon paper down to 2400 micro grit size. The final thickness of the specimens ranges from 0.23 to 0.27 mm. After the punch tests were performed, the sample diameter was always found to remain 3 mm in diameter.

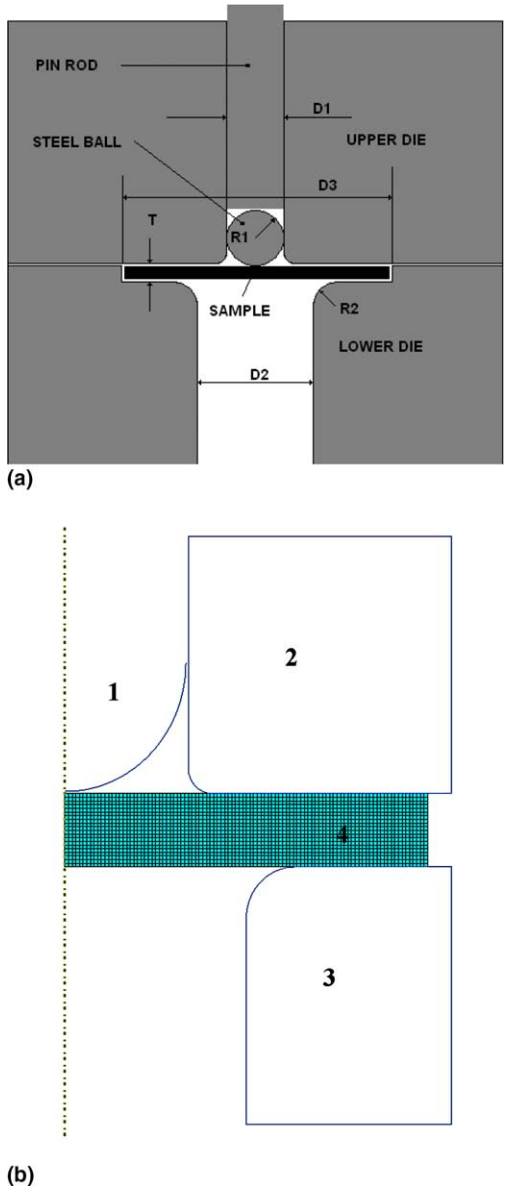

Fig. 1. (a) Sketch of the punch test device showing the more important pieces and dimensions (described in the text). (b) Sketch of the axisymmetric F.E.M. model implemented in ABAQUS for the ball punch test.

3. Finite element modeling

A model for the small ball punch test was developed using ABAQUS 6.4-1 standard code. ABAQUS models

the effect of the multi-axial stress state using the von Mises stress potential and associated J_2 flow law. The model is shown in Fig. 1(b) and includes the ball (1), the upper die (2), the lower die (3) and the sample disk (4). Taking advantage of the rotational symmetry of the experimental set-up, an axisymmetric finite element model was developed. The ball and dies were implemented as rigid bodies. The disk was modeled with 2000 axisymmetric linear reduced integration elements (CAX4R). This element type was selected since it is the most suitable in analysis that involves large strains and strain gradients as well as in contact interaction problems. The number of elements was shown by mesh convergence analysis to be enough to reconstruct properly the load–displacement curves. A force was applied between the upper and the lower dies during the deformation, this prevents the specimen to slip. Friction between these dies and the disk constrains the latter in the same way as in the actual experimental device. The calculations were run by imposing the vertical displacement of the ball. Calculations with frictionless contact interactions as well with a friction coefficient equal to 0.05 between the ball and the disk were considered. Such a friction coefficient is the upper value characterizing the interaction between lubricated polished metal pieces [15]. Finally, a constitutive behavior had to be assigned to the disk. For both steels, the elastic properties, which are the Young's modulus E, the Poisson's ratio ν and the yield stress $\sigma_{0.2}$, defined at 0.2% plastic strain, are summarized in the Table 1. For the plastic behavior, ABAQUS code also requires the plastic behavior represented by the flow stress, σ, as a function of the plastic strain, ε_{pl}, that is written as:

$$\sigma = \sigma_{0.2} + \sigma_{pl}(\varepsilon_{pl}). \quad (1)$$

The $\sigma_{pl}(\varepsilon_{pl})$ equation is derived from the uniaxial tensile behavior. However, this equation can be easily obtained only up to the strain at which the necking starts. However, the equivalent plastic strain at certain locations of the punch disk can reach about 80% in the final stage of the ball punch experiment, i.e., for a strain much larger than the true uniform strain. Hence, it is necessary to extrapolate the tensile curves beyond necking to have the appropriate constitutive behavior used as input in the calculations. Since different extrapolation $\sigma_{pl}(\varepsilon_{pl})$ equations were used in our calculations, we indicate for each of them which constitutive behavior was considered.

Table 1
Elastic parameters for the 316L and F82H-mod steels

Material	E (MPa)	ν	$\sigma_{0.2}$ (MPa)
F82H	207×10^3	0.33	532
316L	207×10^3	0.33	388

4. Results and discussion

4.1. Tensile behavior at room temperature

In Fig. 2, the experimental tensile true stress–true strain curves obtained at room temperature for both steels are plotted up to the stress (strain) at which the necking starts. As expected, significant differences between the tensile properties between these two materials were observed. First, the yield stress of the F82H-mod steel (532 MPa) is higher than that of the 316L steel (388 MPa). Second, the shape of the tensile curve of the F82H-mod presents a more pronounced convex curvature with respect to that of the 316L steel. As a consequence, the true uniform strain is much lower for the F82H-mod, 5% comparatively to that of the 316L, which is 37%. Thus, an extrapolation of the stress–strain relationship to large strains is particularly critical in the case of the F82H-mod steel.

4.2. Ball punch tests at room temperature

The load–displacement curves of two specimens of 316L and F82h-mod steel respectively tested at room temperature are presented in Fig. 3. The thickness of all specimens is 0.23 mm. As can be seen in the Figure, the reproducibility in the experimental curves for both materials is good; the scatter in the load level remains below 5 N for deflection levels below 0.5 mm and increase up to 30 N at the maximum load. There are also some differences to be expected because of the error in the determination of the thickness, around 2 μm, but these are very low. Usually, such a level of reproducibility is reached when problems like improper clamping or initial miss contact between the sample disc and the lower die are solved. Interestingly, the overall shape of the curves for both materials is not identical and differences

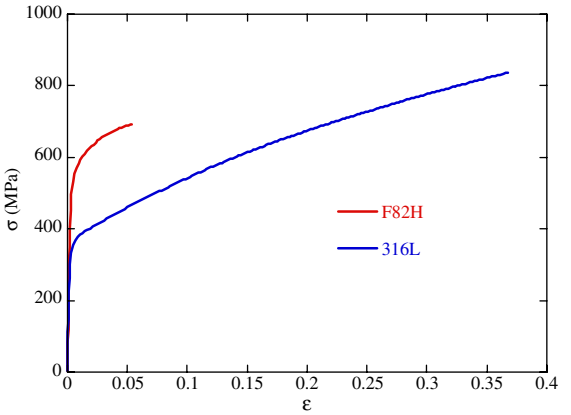

Fig. 2. True stress–true strain tensile tests curves at 293 K for the 316L and F82H-mod steels.

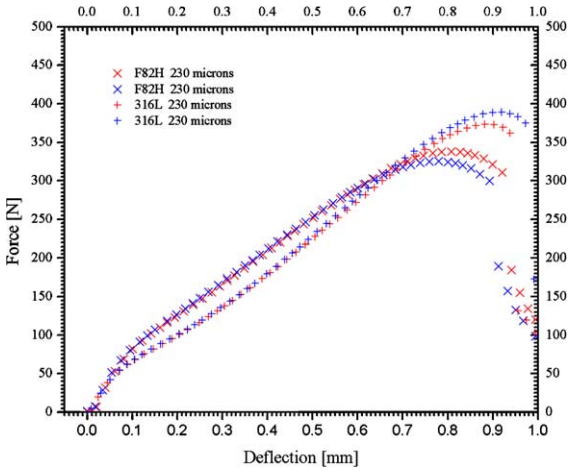

Fig. 3. Experimental reproducibility of ball punch test curves at 293 K for the 316L and F82H-mod steels.

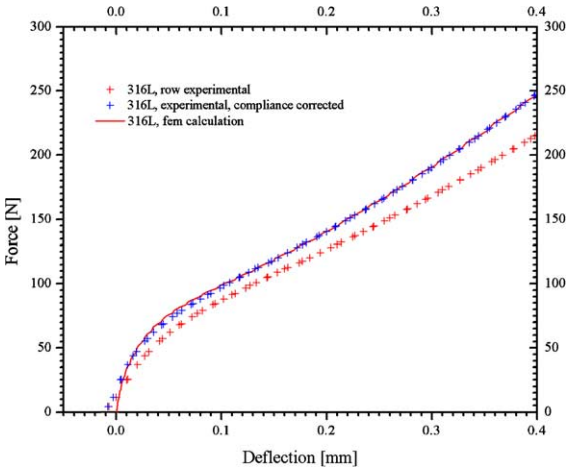

Fig. 4. Effect of compliance correction for small ball punch test at 293 K for the 316L steel.

can be identified. Let us analyze first the 316L steel. For this material, the shape is consistent with what has been observed in the past by other authors [9,16] in austenitic steels. In the Section 4.5, we discuss in details the stress/strain state that develops in the disk as a function of the displacement but we just mention here some authors have associated four deformation regimes to the shape of the curve [5,9,16]. First, the load–displacement curve shows an approximately linear initial loading up to about 40 N, considered as an elastic bending. Second, a plastic bending regime occurs after an extensive yield zone has developed. Third, after the inflection point located around a displacement of 0.35 mm, the deformation mode becomes predominantly membrane stretching and finally, near the maximum load, cracks are expected to develop in the specimen, followed by ductile propagation (in the case of ductile materials), local strain may also occurs as well. The combination of these phenomena results in a decrease in load. As far as the F82H-mod steel is concerned, the above mentioned four deformation regimes cannot be so clearly identified from the shape of the punch test curve, even if the elastic and plastic bending are expected to precede the membrane stretching. In particular, the inflexion point associated to the beginning of the membrane-stretching regime has practically disappeared. Clearly, the difference in the constitutive behavior plays an important role in the shape of the force–deflection curve.

4.3. Ball punch test experiments and finite element calculation validation – 316L steel

The large true uniform strain observed for the 316L steel enables the calculation of a ball punch experiment over a significant displacement range without extrapolating the measured stress–strain relationship deduced from the tensile test. Indeed, it was found that, by using only the $\sigma_{pl}(\varepsilon_{pl})$ data of the tensile test, the calculation can be run up to a displacement of about 0.4 mm while keeping the equivalent plastic strain in the disk mainly below 40%. As a consequence, we start by comparing an experimental and a calculated curve only up to a displacement of 0.4 mm. These two curves are shown in Fig. 4. Two observations have to be done on the experimental curves. First, an initial low-load non-linear regime can bee seen that is likely to be due to a slight initial misalignment of the whole experimental set-up. Second, the initial slope of the calculated curve is clearly steeper than that of the experimental one. Let us mention that, for the calculated curve, the reported displacement refers to that of the ball. This observation suggests that the elastic compliance of the testing device has to be taken into account and that the displacement of the mobile traverse does not represent accurately the one of the ball. This suggestion is also supported by the study of Toloczko et al. [17] done on shear punch tests, where they showed that the elastic loading obtained by finite element analysis are much steeper than that of the experimental curve. Therefore, the experimental load–displacement curves have to be machine-compliance corrected and the following procedure was used. The measured total displacement of the crosshead of the machine (d_{meas}) is the sum of the deflection of the specimen (d_{SP}) and of the elastic displacement of the machine (d_m) so that we can write:

$$d_{SP} = d_{meas} - d_m = d_{meas} - P/K_m, \tag{2}$$

where P is the load and K_m is the machine compliance. Since it is not possible to calculate K_m accurately, it was adjusted by an iterative procedure applied to correct the measured displacement (according to Eq. (2)) until the corrected experimental load–displacement curve

perfectly matches the calculated curve. The compliance corrected curve is presented in Fig. 3, where it can be seen that the calculated curve reproduces very well the experimental one. To gain confidence in the K_m value and then in the correction, several punch test experiments on various materials (austenitic steel, tempered martensitic steels and also Zircaloys) as well as on specimens with different thickness were performed. The experimental curves were compliance corrected using the previously calculated value of K_m. It was found that using the same K_m value for each test, the compliance correction technique shifts systematically all the experimental curves over the calculated ones, independently of the material and thickness. It has to be observed that the initial non-linear low-load region remains poorly fitted by the calculations. Since this non-linear regime is attributed to slight misalignment that necessitates some amount of loading to become negligible, the calculations cannot be expected to yield good results in the initial part of the deformation curve, unless the deflection of the disk is measured with an extensometer touching the bottom of the specimen for example.

Using the finite element model in conjunction with the compliance correction method, three entire experimental curves obtained with different specimen thickness (0.230, 0.250 and 0.270 mm) were calculated. In order to calculate the curves up to deflection larger than 0.4 mm, it was necessary to assign to the disk an extended constitutive behavior. Based upon the observation that the strain-hardening of the 316L steel, defined as $\theta_p = d\sigma/d\varepsilon_p$, has a very low curvature, the stress–strain curve was simply extended linearly above the necking with a strain-hardening rate equal to the value θ_p at the initiation of the necking. The results of the calculations are presented along with the experimental curves in Fig. 5.

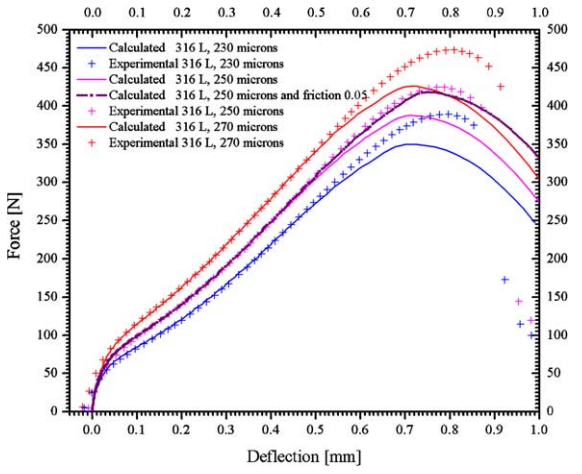

Fig. 5. Experimental and calculated (with and without friction) ball punch test curves at 293 K, for specimens with different thickness of 316L steel.

For each specimen thickness, a good agreement between the experiments and calculations were obtained up to a displacement of 0.5 mm. Beyond that displacement, the experimental data lie systematically above the calculations. A reasonable explanation for this discrepancy is that frictionless interactions have been considered so far. As was shown by Sainte Catherine et al. [18] the introduction of a friction coefficient has practically no effect in the initial part of the loading, but for the last stage the effect becomes more pronounced. Considering a friction coefficient of 0.05, an additional calculation was run. The corresponding calculated curve is presented in Fig. 5, where it can be seen that indeed, the last part of the load–displacement curve is better calculated when a friction coefficient is taken into account. Therefore, the axisymmetric finite element model developed in this work can be considered as satisfactorily validated and can be used to run extensive finite element calculations in order to investigate the influence of other key input parameter like the specimen thickness or the strain-hardening law on the load–deflection curves with a high degree of confidence.

4.4. Ball punch test experiments and finite element calculations – F82H-mod steel

As mentioned above, in the case of the F82H-mod, the limited true uniform strain requires an extrapolation of the stress–strain relationship to larger strain. Therefore, it is of primary importance to use a physically based model for the constitutive behavior to get a certain degree of confidence in the extrapolation. The constitutive behavior of a variety of tempered martensitic alloys has already been investigated at room temperature. It was shown that the strain hardening could be successfully described in the framework of a simplified model of net storage of dislocations with plastic strain [19,20]. In this model, the increase of the post-yield component of the flow stress σ_{pl} scales with $\rho^{1/2}$, where ρ is the total dislocation density. The total dislocation density appears as the only structural parameter of the phenomenological model, which was initially proposed by Kocks and Mecking [21,22]. The net rate of dislocation storage and, consequently, the strain-hardening rate, are mediated by both the mean dislocation displacement distance (before it gets definitely stored into the microstructure) as well as by the mean annihilation distance within which two dislocations can annihilate one another. Therefore, two parameters controlled the strain-hardening rate, P_1, P_2, where P_1 and P_2 are coefficients related to the storage and annihilation of dislocations. In addition, a contribution of the initial dislocation density ρ_0 to σ_{pl} has to be taken into account. Assuming that the high-angle boundaries of the tempered martensitic microstructure constitute impenetrable obstacles for the moving dislocations and that the distance between

those boundaries is strain-independent, it was shown [19] that the following equation described well the post-yield behavior $\sigma_{pl}(\varepsilon_{pl})$ up to the necking:

$$\sigma_{pl} = \sqrt{\frac{P_1 - (P_1 - P_2\sigma_0^2)\exp(-2P_2(\varepsilon_{pl}))}{P_2}} - \sigma_0. \quad (3)$$

The previous equation shows that three parameters have to be fitted to reconstruct the $\sigma_{pl}(\varepsilon_{pl})$ curve, namely P_1, P_2 and σ_0. Note that this equation leads to a saturation stress σ_{sat} at large strain such that $\sigma_{sat} = \sigma_{0.2} + (P_1/P_2)^{1/2} - \sigma_0$. In order to reconstruct the ball punch test curve of a F82H-mod disk with a thickness of 0.23 mm, we ran first a calculation after having assigned to the disk the plastic behavior described by Eq. (3). In Fig. 6(a) we plot the experimental curve along with the calculated one referred to as saturated law. (All the calculated curves in Fig. 6(a) and (b) have been obtained using a friction coefficient equal to 0.05). The two curves start to diverge at a displacement of about 0.3 mm. Comparatively to the calculations done of the 316L steels, a rather small displacement range could be calculated by using the extrapolation of $\sigma_{pl}(\varepsilon_{pl})$ according to Eq. (3). Therefore, the use of this equation to large strain has to be reconsidered. For a displacement of 0.35 mm, there is already a large volume of the disk below the puncher that has undergone an equivalent plastic strain larger than 20%. The extrapolation with Eq. (3) of the $\sigma_{pl}(\varepsilon_{pl})$ to a saturation stress, shown in Fig. 7, indicates that the strain-hardening capacity is reached rapidly. Indeed, the saturation stress, equal to 715 MPa, is practically reached after only 10% of plastic strain. The underestimation of the load–displacement curve resulting from the finite element analysis suggests that the strain-hardening capacity of the material is higher than that

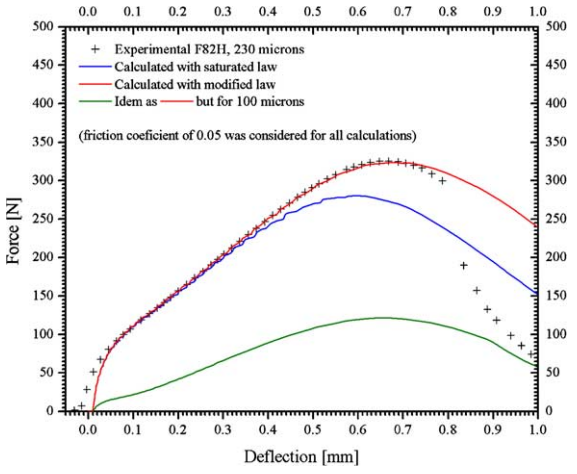

Fig. 6. Experimental ball punch test curve at 293 K for the F28H-mod steel. Calculated curves obtained with different constitutive behaviors (see Fig. 7), and thicknesses.

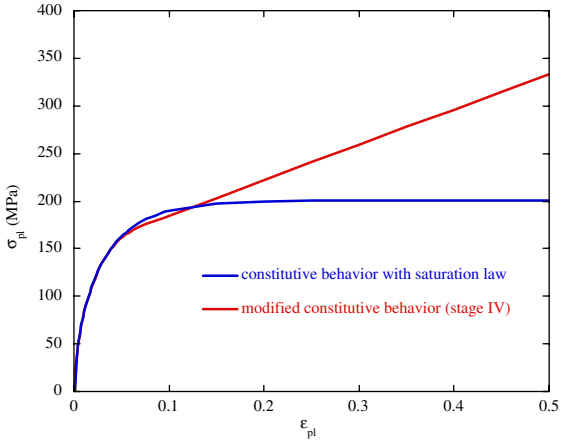

Fig. 7. Assigned constitutive behavior for F82H-mod model steel: (i) stress–strain relationship according to Eq. (2); (ii) consistent with a strain-hardening stage IV.

deduced from Eq. (3). If this is actually the case, the strain-hardening does not decrease monotonously to zero consistently with a stage III of strain-hardening. Rather, it may, at a certain stress (or strain) level, become constant. Thus, another strain-hardening stage has to be considered, which is called stage IV. To our knowledge, no detailed description of the strain-hardening behavior at large strain has been carried out on the 7–9Cr class of tempered martensitic steels. However, there are many investigations in other metals, single and polycrystals as well as pure and technical alloys, where the existence of a strain-hardening stage IV was clearly observed [23–25]. Since the F82H-mod steel has a bcc structure, it is worth mentioning, for similarity at least, that the strain-hardening behavior of an interstitial free and a high strength low alloy ferritic steel, whose structures are also a bcc one, presents a stage IV of deformation [26]. The transition from the stage III to stage IV is usually attributed to important changes in the substructure such as the sub-grain formation, the evolution of the dislocation free path, the cell reorganization or the way the dislocations are stored and annihilated [26]. Introducing a stage IV in the description of the post-yield behavior of the F82H-mod steel is not intrinsically in contradiction with the Eq. (3). We just recall this equation was deduced by assuming a constant mean dislocation displacement distance and a constant dislocation annihilation distance over the entire strain domain. Such an assumption is certainly valid over a limited strain range but the underlying dislocation interaction mechanisms, which have to be little affected by the strain to be in agreement with the assumption, cannot be representative of the actual ones at large strains. While the Eq. (3) can be used to describe the early stage of the tensile curve, the extrapolation to large strain of the tensile behavior with this equation is dubious.

Following the above considerations a second calculation was carried out by assigning a modified constitutive behavior to the disk that is presented in Fig. 7, where it is referred as modified law. The modification consists in extending linearly the flow stress beyond necking. Looking carefully at the Fig. 7, it is obvious that the initiation of the linear regime can take place in a limited strain range, namely between the strain at necking and the strain at which the saturation stress is reached; this corresponds to a strain range of 0.05–0.15, however, this parameter did not have a big influence on the calculated curves. The key point in defining this relationship was the selection of the hardening slope stage IV. It was found that by extending linearly the flow stress from a plastic strain equal to 0.075, the calculated ball punch test curve matches better the experimental curve than that calculated by using a constitutive equation with a saturation stress; this is shown in Fig. 6. Similarly to the calculations done on the 316L steel, it was possible to reconstruct the entire ball punch curve. The modification proposed, referred to as modified law in Fig. 7, should not be taken as the definitive constitutive behavior of the F82h. However, the respective ability of both calculations (with a saturated law of with strain-hardening stage IV) in predicting the experimental ball punch curve clearly indicates that the flow stress does not saturate with strain as rapidly as the Eq. (3) predicts.

4.5. Specimen thickness and constitutive behavior effect on the load–displacement trace

From the experimental point of view, slight thickness variation from specimen to specimen is expected. In Section 4.3, the effect of a thickness variation of ±0.02 mm was illustrated on the calculated curves (Fig. 5), where it can be seen that moderate thickness changes induce a clearly measurable effect on the load–displacement curve. Since we want to extract the maximum amount of constitutive information from the punch test curve, the effect of thickness t_0 has to be taken into account somehow. Calibrations between P_y (P_y is determined by the intersection of the two slopes of the load–displacement curve drawn on both side of the yielding zone) and the yield stress $\sigma_{0.2}$, or the ultimate tensile stress (UTS) and the P_{max} (maximum load on the punch curve) using a normalization of the load of the punch curve by t_0^2, have been proposed by many authors [5,8,9]. In order to check the validity of such normalization, the specimen thickness influence on the overall shape of the punch test traces was studied with calculations for specimens with three significant different thicknesses, namely 0.15, 0.25, 0.35 mm. The 316L steel extended constitutive behavior (linear extrapolation after necking) was assigned to the disk. The results of these calculations are shown in Fig. 8. Interestingly, the shapes of the curves are not self-similar. The traces

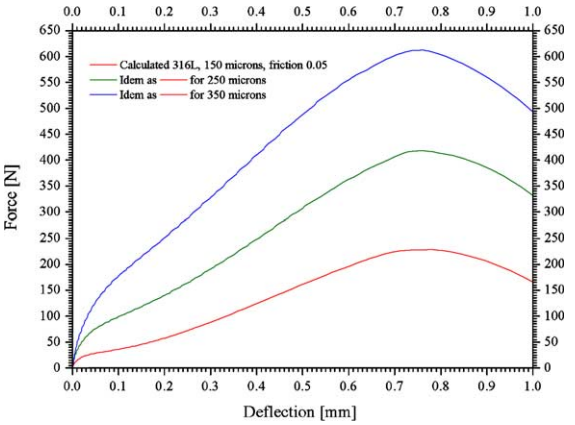

Fig. 8. Specimen thickness influence on the shape of the calculated load–displacement curves, 316L steel.

of the 0.15 and 0.25 mm thick specimens show the four stages mentioned in the Section 4.2. However, increasing the thickness to 0.35 mm leads to a load–deflection curve where the inflection point, associated to the onset of the membrane stretching regime, has disappeared. In Fig. 6, the same observations are also valid for the F82H-mod steel. In this last case, decreasing the thickness from 0.23 down to 0.1 mm results in an overall curve shape change. The direct consequence is that it is not possible to normalize the entire curves by any parameter dependent on t_0 in order to map a set of punch test curves on a self-similar way. Despite the fact that the entire curves cannot be consistently normalized by t_0^2, we found that P_y/t_0^2 yields a value that is reasonably thickness independent. The normalization of P_y is summarized in Tables 2 and 3. From the data presented in these Tables, a correlation of the type $\sigma_{0.2} = \alpha P_y/t_0^2$ confirms that a does not vary notably from one alloy to another as it was observed by [9]. In [9], the coefficient a determined

Table 2
$\sigma_{0.2}$ and P/t_0^2 normalization for the 316L steel

Thickness (mm)	$\sigma_{0.2}$ (MPa)	P/t_0^2 (kN/mm^2)
0.15	388	0.93
0.25	388	1.0
0.35	388	0.99
Averaged values		0.97 ± 0.04

Table 3
$\sigma_{0.2}$ and P/t_0^2 normalization for the F82H steel

Thickness (mm)	$\sigma_{0.2}$ (MPa)	P/t_0^2 (kN/mm^2)
0.1	532	1.3
0.23	532	1.45
Averaged values		1.37 ± 0.08

for a variety of material was found equal to 360 MPa/(kN/mm^2). In our case, the a coefficients that are obtained at room temperature for the 316L and F82H-mod steel, respectively, are 400 ± 12 and 388 ± 22 MPa/(kN/mm^2).

In order to check that P_y is really mediated by the yield stress, we ran two extra calculations; they are not shown in Fig. 6 to avoid confusion. First, an 'hybrid' calculation, where the constitutive behavior of the material is such that the yield stress corresponds to that of the F82H-mod steel and the $\sigma_{pl}(\varepsilon_{pl})$ relationship is that of the 316L steel. The result of this calculation showed us that, up to a displacement of about 0.3 mm, the punch test curves are not strongly affected by the post-yield behavior. However, its effect becomes noticeable at larger displacements (the 'hybrid' calculation lies on the top of the curve for the F82H up to deflections <0.3 mm and then deviates to higher force levels). Second, in order to show the difference between a strain-hardening material and a material with a flow stress almost equal to the yield stress, a calculation with an almost perfectly plastic material (increase of 25 MPa over 100% plastic strain) was done. The calculated curve, although possessing the same P_y, lies well below the other ones obtained with the strain-hardening materials. So it can be concluded that P_y is only affected by the yield stress of the material.

Further in this thickness effect analysis, we show in Fig. 9 the equivalent plastic strain contour plots for the 316L steel at a ball deflection level of 0.1 mm and for two disk thickness (0.15, 0.35 mm). For both thicknesses, the total displacement of the ball can be split into two contributions: (i) a plastic displacement due to an indentation like plastic zone at the ball tip; (ii) an elastic bending localized between the limit of the plastic zone and the contact with the lower die. It can be seen that the total displacement of the ball for the thicker specimen is mainly accommodated by the indentation plastic flow; the elastic bending remaining small. On the contrary, for the thinner specimen, the elastic bending contribution dominates. We recall that for the 0.35 mm thick specimen, the load–displacement curve presents three stages instead of four, there is single linear regime above the macro yielding. Another contour plot for a 0.23 mm thick disk of F82H-mod steel is shown for the same deflection of the ball in Fig. 10. In this last example, the splitting of the total displacement constitutes an intermediate situation where the plastic deformation and elastic bending contribution are comparable. In this last case, a single linear regime was also observed after the macro yielding. Thus, it is concluded that a separation between a – so-called – plastic bending and membrane-stretching regime is more pronounced when a well dominated elastic bending regime occurs in the initial stage. For the F82H-mod this is again the case for a thickness of 100 μm as shown by the FEM calculations in Fig. 6. The corresponding contour plots are also shown in Fig. 10. Hence, one should not always expect four regimes force–deflection curves in small ball punch test. For a given material the four regimes are always found for thin enough samples. Along this line of thinking, if the thickness is kept fixed, the four regimes will show up for materials with comparatively low yield stress and high hardening rate. Note in Figs. 9 and 10 that in both cases the thinner specimens show micro yielding in tension near the bottom surface of the sample disc, while the thicker ones in compression near the top surface, consistently with a preponderance of the indentation. Finally, let us mention that owing to the geometry of the ball punch test, the first deformation stage cannot be really regarded as purely linear elastic because there is always micro yielding at the punch tip. On the load–displacement curves, this behavior is consistent with the fact that the load–displacement curves always show some curvature at low load. This induces some uncertainty in the determination of P_y since determining a straight line before the extensive yielding is a matter of judgment. However, the resulting error in the determination of P_y remains however of the order of 5%.

Regarding the proposed calibrations between P_{max} and the ultimate tensile stress, we make the following remarks: It can be seen that our FEM model leads to a decrease of the load level at deflections around 0.7 mm *when friction is taken into account*. Thus, for the two materials presented, P_{max} as well as the deflection level for which it occurs are rather well estimated by the FEM calculation. Nevertheless, special care should be taken for two reasons: (i) punch test experiments we performed on Zircaloy and aluminum alloys of the same geometry (not shown in this work) show considerably lower values for the deflection at P_{max}, around 0.4 mm. However, some calculations already ran for Zircaloy, although reproducing satisfactorily the first stages of the force deflection curve, show similar levels for P_{max} as for the materials presented here, in disagreement with the experimental curves; (ii) other authors working with austenitic steels have shown [27] that there are clearly visible microcraks at deflection levels well below the maximum load is reached. Obviously, our FEM model does not consider this process. Note (Fig. 3), that the experimental determination of P_{max} is subjected to considerable scatter, of the order of 30 N. Thus, for the range of sample thickness normally employed, a t_0 or a t_0^2 normalization of P_{max} cannot be decided. Furthermore, correlating P_{max} with the UTS and the displacement at maximum load with the uniform elongation remains an open issue.

4.6. Applicability of the punch test for irradiated material

In the previous sections, we have shown that, in spite of the complex stress/strain state that appears from the

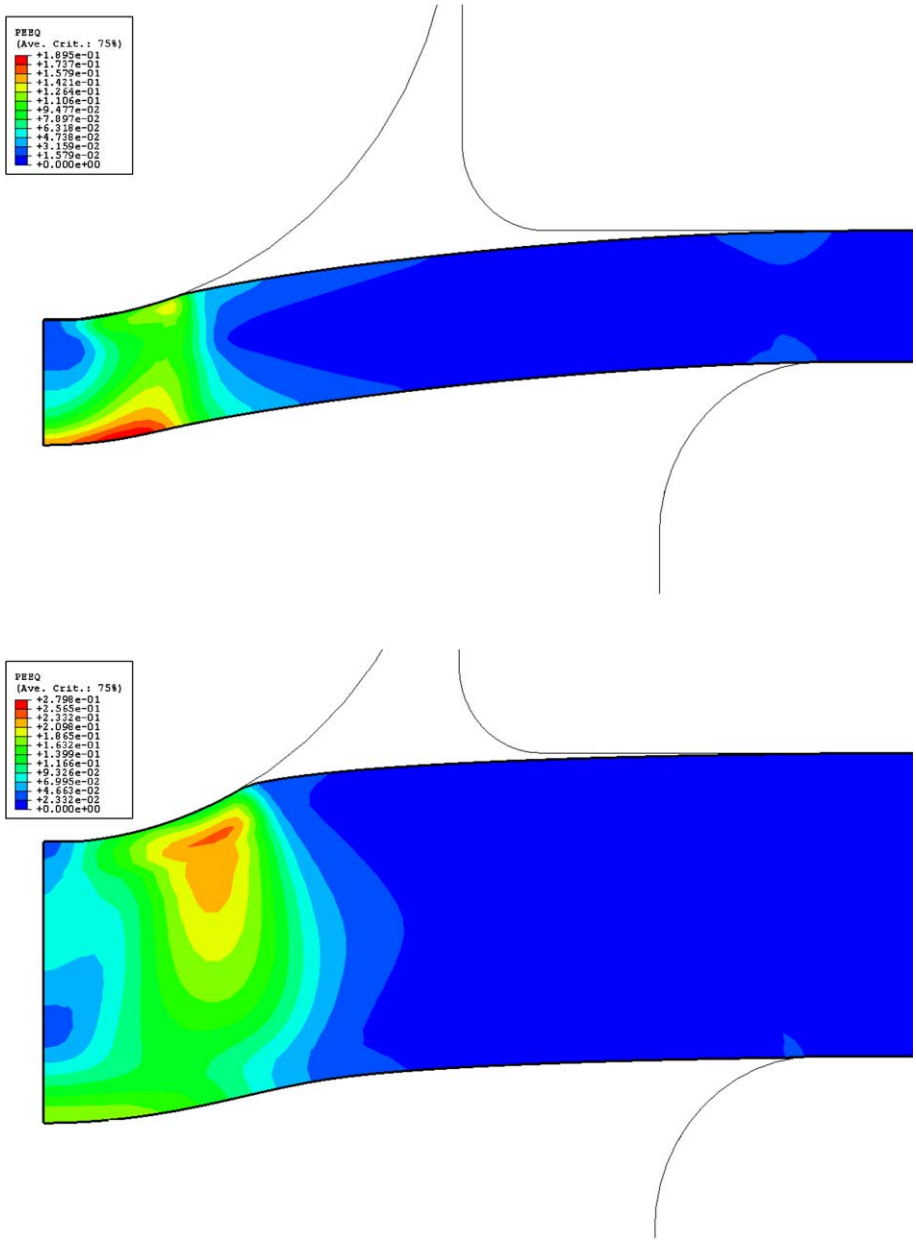

Fig. 9. Equivalent plastic strain contour plots for the 316L steel for two disc thicknesses (0.15 and 0.35 mm) at a ball deflection of 0.1 mm.

very beginning of the ball punch experiment, critical information can be reliably extracted from such tests when the experimental data are supplemented with finite element calculations. In particular, the constitutive behavior of a given material used in a punch test simulation can be estimated iteratively until the calculated load–displacement curve matches the experimental one. Let us emphasize again that, as long as the material plastic behavior is isotropic (see below), there is a unique $\sigma(\varepsilon)$ relationship that allows reconstruction of the experimental punch test curve. This observation makes the finite element modeling of the punch test experiments quite attractive to gain insights into the constitutive behavior up to large strain of irradiated materials, since the $\sigma(\varepsilon)$ relationship can be derived from the simulations. Indeed, the stress/strain relationship for irradiated materials like the tempered martensitic steels or V–4Cr–4Ti alloys for example, cannot be obtained by tensile

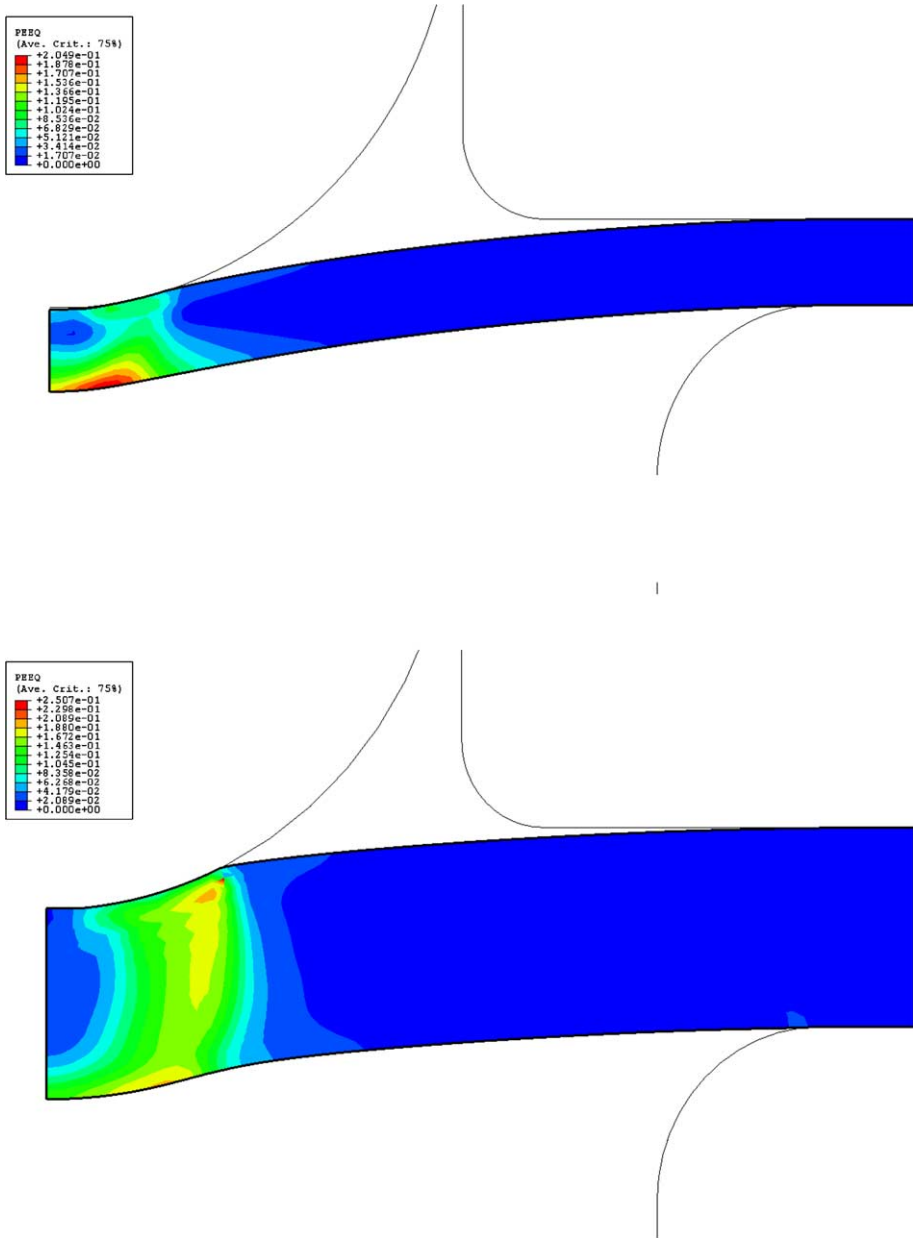

Fig. 10. Equivalent plastic strain contours plots for the F82H-mod steel for 0.23 and 0.1 mm thickness at the same ball deflection.

tests since these alloys exhibit a very limited uniform strain after irradiation, which is actually the direct consequence of the irradiation hardening reflected in a yield stress increase [28]. This prevents studying their strain-hardening evolution under irradiation with tensile tests. However, adjusting the constitutive behavior to fit the experimental punch curves will require special attention. It is well established that in many metals and alloys irradiation induces an increase of the yield stress followed by a yield drop or moderate strain softening before the material recovers its strain-hardening capacity [29]. The whole process can be associated to a complex mode of plastic deformation that occurs partly in strain-softening channels and partly in a strain-hardening matrix; the materials can then be regarded as composite materials made of soft and hard regions [28]. The $\sigma(\varepsilon)$ curve for such a material has to be understood as a representation of a volume weighted average of the constitutive properties of the soft and hard regions and the shape of the curve cannot be represented any more by a single

relationship of the type of the Eq. (2). Therefore, adjusting the $\sigma(\varepsilon)$ curve to reconstruct the punch curve of irradiated materials is a more complicated task than just adjusting the parameters of the Eq. (3) and the slope of the stage IV but the strain-softening domain after the yield stress and the strain-hardening that follows after a certain amount of strain have to be taken into account. Owing to this more complex nature of the plastic flow properties in the irradiated material than in the unirradiated one and to the many parameters to be fitted, it is anticipated that additional testing is necessary if the constitutive behavior at large strain has to be established in a reliable manner. Typically, for irradiated materials compression tests could be used to get the constitutive behavior from low to moderate strains. Let us finally mention that, if only the irradiation hardening has to be measured (increase of the yield stress), the calibration between P_y/t_0^2 and $\sigma_{0.2}$ done on the unirradiated materials can still be used for the irradiated materials since it was shown to be post-yield behavior independent.

Regarding the assessment of the constitutive behavior for anisotropic materials like zirconium or titanium alloys, it will be shown in a continuation of this article that the punch test force–deflection curve does not follow uniquely from a given constitutive behavior, since it is then possible to vary simultaneously the parameters that model the hardening and the anisotropy in such a way that the correct force deflection curve (up to the experimental error) is reproduced for more than one set of these parameters. However, in this case it is possible to complement the punch tests with other kind of non-standard tests in order to reduce further the choice of parameters that are able at reproducing both experiments at the same time.

5. Concluding statements

Small ball punch tests and tensile tests have been carried out at room temperature on a 316L steel, as well as on the F82H-mod tempered martensitic steel. In order to extract the constitutive behavior from the ball punch test, a finite element model has been developed and validated. The effects of load-train compliance, of the yield stress, of the post-yield behavior, of the specimen thickness, of the ball-specimen friction have been investigated in details. The results can be summarized as follows:

(i) Significant differences in the tensile behavior of the two steels were found. The yield stress of the F82H-mod steel is larger (532 MPa) than that of the 316L steel (388 MPa) but the uniform elongation is much lower for the F82H-mod (5%) than for the 316L (37%).

(ii) The finite element model for the small ball punch test was validated with the 316L steel because the constitutive behavior determined by tensile tests allows calculations up to a relatively large displacement of the ball, about 0.4 mm, without introducing additional assumption on the constitutive behavior. Indeed, at such a displacement, the equivalent plastic strain in the disk remains below 40%, i.e., almost the same as the true uniform strain.

(iii) The calculations showed that the load–displacement compliance is not negligible and has to be taken into account. Since the experimental curves were obtained by measuring the displacement of the testing machine crosshead, they had to be compliance corrected before comparison with the calculations. It is then desirable to avoid the compliance correction by measuring the deflection of the specimen with an extensometer touching the bottom part of the disk. Furthermore, this is particularly important in the case irradiated materials for which the post-yield behavior cannot be obtained over a broad range of strains by tensile tests and where an inverse methodology to determine the true stress–true strain relationship will have to be used to reconstruct the punch test load–displacement curve.

(iv) In order to calculate properly the entire punch curves up to the maximum load, it was necessary to consider a small friction effect between the ball and the disk. The friction effect becomes apparent only for displacement larger than 0.5 mm and is reflected by an increase of load with respect to calculation where no friction is considered.

(v) The overall shape of the punch curve was discussed as a function of the specimen thickness and of the constitutive behavior. Depending on the combination of these last two parameters, three or four deformation stage could be identified. The shape of the punch curve results from a combination of the micro-indentation at the ball tip, elastic + plastic bending and membrane stretching. The relative contribution of these various processes as deformation proceeds actually controls the shape of the curve.

(vi) Based upon calculated punch curves on different thicknesses for both steels, the usual correlation between the thickness normalized yield load value P_y/t_0^2 of the punch experiment and the yield stress was verified. However, it was demonstrated that the entire curve cannot be normalized by P_y/t_0^2. Furthermore, we do not believe that correlating the maximum load to the ultimate tensile stress is really representative of a physical mechanism since the averaged equivalent stress/strain state at maximum load is totally different from that at necking.

(vii) The punch test calculations of the F82H-mod steel were found to match the experimental curve only when using a stress–strain relationship whose strain-hardening is separated into two stages that can be phenomenologically described as a stage III and IV. As a matter of fact, this is a typical example of the potential of the punch test in evaluating the strain-hardening at large strain. By extension of the technique to the irradiated material, it is expected to get a reasonable assessment of the strain-hardening behavior after irradiation by adjusting a $\sigma_{pl}(\varepsilon_{pl})$ curve in the input of the calculation, using an inverse methodology.

Acknowledgments

The financial support of Swiss Nuclear and EURATOM, respectively, is acknowledged, also the technical support of A. Kramer and the assistance of many colleagues at PSI for valuable suggestions and discussion on the manuscript.

References

[1] W.R. Corwin, G.E. Lucas (Eds.), The Use of Small-scale Specimens for Testing Irradiated Material ASTM-STP 888, American Society for Testing and Materials, Philadelphia, PA, 1986.
[2] G.E. Lucas, J. Nucl. Mater. 177 (1983) 327.
[3] P. Jung, A. Hishinuma, G.E. Lucas, H. Ullmaier, J. Nucl. Mater. 232 (1996) 186.
[4] G.E. Lucas, G.R. Odette, M. Sokolov, P. Spätig, T. Yamamoto, P. Jung, J. Nucl. Mater. 301–311 (2002) 1600.
[5] E. Fleury, J.S. Ha, Inter. J. Pressure Vessels Piping 75 (1998) 699.
[6] J.S. Ha, E. Fleury, Inter. J. Pressure Vessels Piping 75 (1998).
[7] A.N. Sinclair, O. Lepik, M. Gabbani, B. Mukherjee, E. Alberti, in: W.R. Corwin, F.M. Haggag, W.L. Server (Eds.), Small Specimen Test Techniques Applied to Nuclear Reactor Vessel Thermal Annealing and Plant Life Extension, ASTM STP 1204, American Society for Testing and Materials, Philadelphia, PA, 1993, p. 162.
[8] Y. Ruan, P. Spätig, M. Victoria, J. Nucl. Mater. 307–311 (2002) 236.
[9] X. Mao, H. Takahashi, J. Nucl. Mater. 150 (1987) 42.
[10] J. Kameda, X. Mao, J. Mater. Sci. 27 (1992) 983.
[11] J. Lee, I. Kim, A. Kimura, J. Nucl. Sci. Technol. 40 (2003) 664.
[12] P. Fernandez, et al., J. Nucl. Mater. 307–311 (2002) 495.
[13] A. Hishinuma, A. Kohyama, R.L. Klueh, D.S. Gelles, W. Dietz, K. Ehrlich, J. Nucl. Mater. 258–263 (1998) 193.
[14] R. Bonadé et al., to be published.
[15] A. Olza, F. Taillard, E. Vautravers, J.C. Diethelm, Tables Numériques et Formulaires, Ed. SPES, 1978, p. 243.
[16] G.E. Lucas, A. Okada, M. Kiritani, J. Nucl. Mater. 141–143 (1986) 632.
[17] M. Toloczko, K. Abe, M.L. Hamilton, F.A. Garner, R. Kurtz, Mater. Trans. JIM 41 (2000) 1356.
[18] C. Sainte Catherine, J. Messier, C. Poussard, S. Rosinski, J. Foulds, in: M.A. Sokolov, J.D. Landes, G.E. Lucas, (Eds.), Small Specimen Test Technique, vol. 4, ASTM STP 1418, American Society for Testing and Materials, West Conshohoken PA, 2002, p. 350.
[19] R. Bonadé, P. Spätig, R. Schäublin, M. Victoria, MSE A, in press.
[20] R. Bonadé, P. Spätig, M. Victoria, T. Yamamoto, G.R. Odette, J. Nucl. Mater. 329–333 (2004) 278.
[21] U.F. Kocks, J. Eng. Mater. Tech. (ASM H) 98 (1976) 41.
[22] H. Mecking, U.F. Kocks, Acta Metall. 29 (1981) 1865.
[23] J. Gil-Sevillano, E. Aernoudt, Mater. Sci. Eng. 86 (1987) 31.
[24] M. Zehetbauer, V. Seumer, Acta Metall. 41 (1993) 577.
[25] P.N.B. Anongba, J. Bonneville, J.-L. Martin, Acta Metall. Mater. 41 (1993) 2897.
[26] X.F. Fang, W. Dahl, Mater. Sci. Eng. A 203 (1995) 14.
[27] M.P. Manahan, A.E. Browning, A.S. Argon, O.K. Harling, in: W.R. Corwin, G.E. Lucas (Eds.), The Use of Small-scale Specimens for Testing Irradiated Material, ASTM-STP 888, American Society for Testing and Materials, Philadelphia, PA, 1986, p. 17.
[28] G.R. Odette, M.Y. He, E.G. Donahue, P. Spätig, T. Yamamoto, J. Nucl. Mater. 307–311 (2002) 171.
[29] B.N. Singh, N.M. Ghoniem, H. Trinkaus, J. Nucl. Mater. 307–311 (2002) 159.